Combustion and Flame 163 (2016) 179–187

Contents lists available at ScienceDirect

Combustion and Flame

journal homepage: www.elsevier.com/locate/combustflame

Soot oxidation-induced fragmentation: Part 1: The relationship between soot nanostructure and oxidation-induced fragmentation

Hossein Ghiassi [a,*], Pal Toth [b], Isabel C. Jaramillo [a], JoAnn S. Lighty [a]

[a] Department of Chemical Engineering, University of Utah, Salt Lake City, Utah, USA
[b] Department of Combustion Technology and Thermal Energy, University of Miskolc, Miskolc, Hungary

ARTICLE INFO

Article history:
Received 16 April 2015
Revised 3 September 2015
Accepted 3 September 2015
Available online 19 November 2015

Keywords:
Soot oxidation
soot fragmentation
Internal burning
Aggregate break up
Image analysis

ABSTRACT

This paper tests the proposed mechanisms in the literature [1] where the fragmentation was suggested to be as either the result of aggregate break up due to preferential burning in the bridge sites or the result of primary particle fragmentation due to internal burning. In order to evaluate aggregate break up, high-resolution transmission electron microscopy (HR-TEM) images were analyzed to compare the soot nanostructure of the bridge sites with the particle sites. Results demonstrated that the bridge sites were formed by less-ordered nanostructure indicating a higher oxidation potential than particle sites. In addition, the feasibility of internal burning in the single particles was tested through an analysis of intraparticle diffusion. In this case, the actual oxygen diffusion pathway as well as effective spacing between the crystalline structures was estimated by the image analysis technique. By using the obtained data in the effectiveness factor calculation, it was found that the possibility of internal burning by O_2 molecules increased for particles less than 10 nm as compared to larger particles. In addition, increasing temperature decreased the potential for internal burning.

1. Introduction

The term "soot nanostructure" has been used broadly to refer to the physical properties such as dimensions and relative orientations of the graphene-like segments in soot particles [2]. High-Resolution Transmission Electron Microscopy (HR-TEM) is a suitable approach to characterize the nanostructure of soot samples [2–7]. It has been shown that initial fuel type and synthesis conditions of temperature and time affect the soot nanostructure [8]. Several studies have been performed to explore the effect of nanostructure on the soot oxidation rate [3,9,10]. A considerable number of them have been devoted to systems where oxygen is the oxidizer [15,25,30].Vander Wal and Tomasek [9] studied the differences in nanostructure and reactivity for soot samples generated from benzene, ethanol and acetylene. Their results showed that soot from benzene with amorphous structure and from ethanol with curvy plane layers was more reactive than the sample from acetylene with a graphitic-like structure. In another study, Vander Wal and Muller [16] confirmed that the soot nanostructure comprised of either curvy or disordered structures showed a higher reactivity toward oxidation. Su et al. [14] used HR-TEM and TGA to correlate the nanostructure with oxidation reactivity of different soot samples from exhaust of heavy duty (HD) diesel engines. Yehliu et al. [9] suggested that oxidative reactivity is primarily dominated by the disordered carbonaceous structure. Jaramillo et al. [2] determined the kinetic parameters for soot oxidation by using TGA for several pure component hydrocarbon fuels and surrogates. They also investigated the role of nanostructure in the oxidation of the soot samples. Their result demonstrated that the activation energy is proportional to the fringe length and inversely proportional to the fringe tortuosity.

In a flame study, where *OH* was the main oxidizer, Ghiassi et al. [11] investigated the role of nanostructure on the soot surface reactivity. The fringe orientation maps were quantified in terms of polar (a representative of curvy structure) and nematic (a representative of flat structure) symmetry, as illustrated in Fig. 1. The oxidative reactivity was shown to be correlated with the degree of orderliness of layer planes. The most reactive soot had an amorphous nanostructure which was composed of short individual layer planes with no orientation relative to each other. For this type of nanostructure, the higher ratio of carbon in the edge sites versus basal plane sites implied a higher oxidative reactivity. With the same layer plane size, higher relative curvatures were more reactive. Indeed, the curvature weakens the C–C bond and makes it more susceptible to oxidative attack by imposing bond strain and reducing electronic resonance stabilization in the orbital overlap [9,12].

Soot fragmentation has been hypothesized with two sub-mechanisms [13]: (i) O_2 penetrating the primary soot particles, which in turn, causes internal burning and loss of the connectivity between

* Corresponding author.
E-mail address: hosseinghiassi@yahoo.com (H. Ghiassi).

http://dx.doi.org/10.1016/j.combustflame.2015.09.023
0010-2180/

Abbreviations

C_{O2}	Oxygen concentration ($\frac{mol}{cm^2}$)
D_K	Knudsen diffusion coefficient ($\frac{cm^2}{s}$)
D_e	Effective diffusion ($\frac{cm^2}{s}$)
k'	Rate constant ($\frac{cm^3}{cm^2 \cdot s}$)
k	Rate constant ($\frac{1}{s}$)
M	Oxygen molecular weight
M_T^2	Modified Thiele Module
R	Radius of soot particle
R_g	Universal gas constant
r_p	Effective pore space
S_{BET}	BET surface ($\frac{m^2}{gr}$)
T	Temperature (K)
t_D	Diffusion time scale (s)
t_r	Reaction time scale (s)
W	Soot oxidation rate ($\frac{gr}{cm^2 \cdot s}$)
Greek symbols	
τ	Tortuosity
γ	Soot porosity
ρ	Soot density
η	Effectiveness factor

the carbonaceous phases, results in breaking up of primary particles (ii) the breakup of bridges (or necks) between primary particles in the aggregate structure and the removal of small fragments from the edges of the primary particles surface. In this study, these two mechanisms are examined. To explore the reactivity of the bridge sites between two particles, the nanostructure was quantified by image analysis and compared to the nanostructure of bulk materials. In addition, the possibility of internal burning of primary particles was tested by comparing the diffusion time scale to reaction time scale through the effectiveness factor analysis. The parameters needed to calculate the effectiveness factor including the actual oxygen diffusion pathway and pore width were estimated by the image analysis technique.

2. Experimental set-up

In order to investigate the morphology and nanostructure of the different soot samples, HR-TEM was performed. Soot was generated in a two-stage burner [11,13,14]. The soot sample was deposited on a lacey C/Cu TEM grid following the procedure of thermophoretic sampling by Dobbins [15]. TEM grids were rapidly inserted in the flow of combustion gases and soot was deposited due to the thermophoretic gradient. Multiple insertions were used to get a proper representative sample on the grid. A TEM grid holder attached to a piston and compressed air at 60 psig was used to quickly insert the TEM grid into the flame to minimize the impact of flame temperature on the particles that experienced multiple insertions [16]. The temperature of the carrier probe during the sampling was measured by attaching a thermocouple (type B) on the top of the TEM holder. The carrier probe reached a local maximum temperature as high as 450 ± 10 K while at the same HAB the flame temperature was around 1500 K. This confirmed the minor temperature effect on the soot samples on the grid. In addition, the control system was designed to move the probe with the maximum speed to a precisely defined position in the flame. Figure 2 shows the schematic diagram of the probe control system. The soot grid samples were taken from the second burner at initial heights where soot did not undergo any oxidation reactions. The precise spatial positioning of the probe within the flame was achieved by mounting the mechanical components on a translation stage. The accuracy of probe positioning was estimated to be better than 0.1 mm. TEM images were taken using a FEI Tecnai F20 Ultratwin TEM/STEM operating at 200 keV.

TEM images were processed by an image analysis framework designed for quantifying the soot nanostructure [17–19]. The framework is based on filtering theory in order to extract the symmetry parameters. Nematic and polar order parameters (S_{2N} and S_{2P}, respectively) introduced by Shim et al. [20] were extracted by the orientation-filtering technique developed by Toth et al. [18]. Polar symmetry quantifies the dominance of fringes oriented concentrically around a symmetry pole in the overall structure. The nematic symmetry strength parameter quantifies the prevalence of flat graphene layers (graphite-like microcrystals) in the structure. In general, high values of both symmetry parameters imply graphite-like nanostructure. With the method utilized here, it is possible to describe the symmetry of the structure over multiple spatial scales. The bridge sites in the aggregate structure were identified manually, based on which image masks were defined, locating pixels that belonged to bridge sites. The symmetry parameters computed over the masked areas were compared to those computed over the rest ("bulk") of the imaged structures.

During the assessment of the possibility of internal burning, the knowledge of actual distance travelled by O_2 molecules toward the center of a particle before reacting with an active site is needed. The image analysis procedure similar to that described by Toth et al. [19] was utilized to estimate this. In brief, sub-structures with high nematic symmetry strength were detected by setting a threshold on S_{2N} and constructing binary images that contained true values at the detected patches of high nematic symmetry. The remaining (unmasked) areas represented amorphous material, characterized by low S_{2N} values. It was postulated that O_2 molecules only diffuse through the amorphous phase, as the porous structure imposes much less diffusion resistance as compared to the fairly crystalline sub-structures.

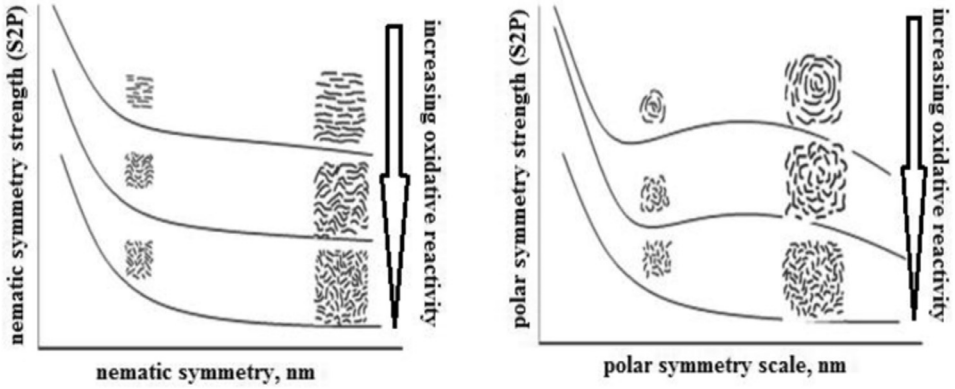

Fig. 1. Histogram of symmetry strength versus symmetry scale for nematic symmetry (left) and polar symmetry (right) which was in correlation with soot oxidative reactivity [11].